Numerical Computation of In-cell Parameters for Multiwire Formalism in FDTD

Jesper Lansink Rotgerink[#1], Harmen Schippers[#2], Alberto Gáscon Bravo[*3], Luis D. Angulo[*4], Salvador G. García[*5]

[#]Royal Netherlands Aerospace Centre (NLR), the Netherlands

[*]University of Granada, Spain

{[1]Jesper.Lansink.Rotgerink, [2]Harmen.Schippers}@nlr.nl, {[3]agascon, [4]lmdiazangulo, [5]salva}@ugr.es

***Abstract* — The finite-difference time-domain method is a very suitable tool to analyse the propagation of, among others, lightning and arcing through new high voltage high power distribution networks in aircraft. This paper presents a numerical method for the computation of the in-cell inductance and in-cell capacitance matrices, required to accurately model wire bundles in a finite-difference time-domain grid. The method extends the multiwire formalism proposed by Bérenger, and enables the inclusion of inhomogeneous media, as well as non-cylindrical conductors. Moreover, the method accurately computes the interactions between closely spaced wires that are neglected by the analytical formulation of Bérenger. The presented method is applied to a testcase that can be compared to Bérenger's results. Finally, results for a testcase that involves dielectric insulation are given.**

***Keywords* — finite-difference time-domain, electromagnetic compatibility, transmission lines, in-cell parameters.**

I. INTRODUCTION

The significant developments towards hybrid or full electric aircraft in a quest for emission-free aviation, require redesign of on-board power distribution networks. In the Clean Aviation project HECATE (Hybrid ElectriC regional Aircraft distribution Technologies), critical enabling technologies for a power distribution network of a regional hybrid electric aircraft are being developed. The increased power and voltage levels in such power networks pose risks in terms of electromagnetic compatibility (EMC). These include the challenges to the cabling in terms of arcing, crosstalk, radiated emissions, as well as lightning induced effects (LIE). Solutions will be sought for these challenges within the HECATE project. In this project, the University of Granada is developing the SEMBA-UGRFDTD simulation tool, which contains as a module a parallel-computing finite-difference time-domain (FDTD) solver [1]. In the HECATE project this tool will be extended to analyse EMC aspects of new cabling concepts for power distribution networks that can safely handle the high power and high voltage levels occurring in future hybrid electric aircraft.

Simulation tools are generally very useful in the analysis of EMC challenges in aircraft. Frequency domain multiconductor transmission line (MTL) simulations are frequently performed to investigate for instance crosstalk or radiated emissions for the electrical wiring interconnection system (EWIS) in aircraft [2]-[5]. However, time domain methods may be more efficient in case transient effects, such as propagation of arcs or lightning induced effects through an HV network, are to be analysed. The FDTD method is a widely used computational method for electromagnetic analysis of large structures such as aircraft and naval platforms [6]. However, it is challenging to model wires in the FDTD method, because the diameters of wires are usually much smaller than the cell size of FDTD computational grids. To allow any wire to be included, the single thin wire formalism has been introduced by Holland [7]. This has been generalized to a multiwire formalism by Bérenger [8], and later extended to include for instance oblique and shielded wires [9], [10]. However, the focus of this paper will not be on the FDTD implementation itself, but rather on the derivation of required in-cell parameters. The formalism for that as presented by Bérenger [8] takes into account bundles composed of parallel wires, with the advantage that the wire bundle cross section is inside one FDTD cell. Assuming static magnetic and electric fields around infinitely long wires with uniform charge, Bérenger has derived analytical formulas for the inductance and capacitance of the wires inside one FDTD cell, referred to as the in-cell inductance and capacitance.

In this paper, Bérenger's method will be generalized, so that EMC transient effects of new cabling concepts for high power distribution networks can be accurately analysed. This new cabling is characterized by insulated wires with several thicknesses, which can be located close to each other. Compared to the generalization in this paper, Bérenger's formulation has some drawbacks. First of all, it will be shown that the coupling between the wires in the Bérenger formulation is weak. For the testcase consisting of one thin wire (with diameter 1 mm) and one thick wire (with diameter 10 mm) it will be shown that Bérenger's analytical approach neglects certain interactions between these wires. Another disadvantage of Bérenger's formulation is its restriction to cylindrical wires embedded in a single, homogeneous medium. Thus, it cannot take into account insulation around wires, i.e. inhomogeneous media.

The generalization presented in this paper will focus on the derivation of the in-cell inductance and capacitance matrices from a numerical Laplace solver, by means of the finite element method (FEM). While a clear drawback may be in longer required computation time, this new method enables the computation of the required matrices for any cabling configuration, with neither any assumptions on size, thickness and separation of wires, nor homogeneous media. Additional

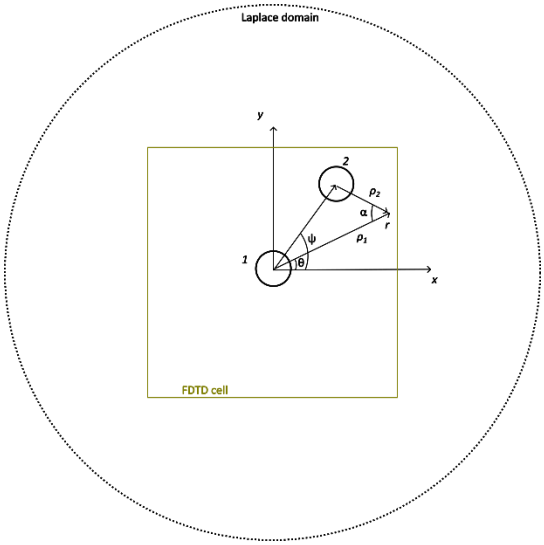

Fig. 1. Sketch of two wires inside an FDTD cell. Outer circle illustrates the outer boundary of the FEM domain.

benefit of such a numerical computation of in-cell parameters, is the ability to solve also for cables having non-cylindrical cross section (for instance busbars and rectangular traces on a PCB). A solution to include dielectric insulation into the analytical expressions of Bérenger has been presented in [10]. It is shown that the effects of such insulation can also be included in the numerical computation of in-cell parameters by the NLR Laplace solver. For the testcase concerning one thick and one thin wire, which can be computed both numerically and analytically, results of the in-cell parameters will be compared. These will be used in an FDTD solver to validate their outcomes against the literature. Finally, this paper will also illustrate how to deal with additional technicalities of insulation around wires involving the coupling equations between the wires and FDTD.

The following Section will briefly summarize Bérenger's multiwire formalism, so that in Section III the expansion towards numerical computation of in-cell parameters can be introduced. In Section IV results of simulation will be given. Finally, Section V will give conclusions.

II. Bérenger's Multiwire Formalism

Consider two wires with radii a_1 and a_2 inside a single FDTD cell, in which wire 1 is located at the origin, as shown in Fig. 1. A charge per unit length (p.u.l.) on each of these wires, Q_1 and Q_2 respectively, will cause an electric field at given a distance ρ_1 from the origin:

$$E_r(\rho_1) = \frac{Q_1}{2\pi\varepsilon_0\rho_1} + \cos\alpha\,\frac{Q_2}{2\pi\varepsilon_0\rho_2}. \tag{1}$$

Integrating this over ρ from a_1 to a distance r yields the potential between the centre wire and point r:

$$V(r) = \frac{Q_1}{2\pi\varepsilon_0}\ln\left(\frac{r}{a_1}\right) + \frac{Q_2}{4\pi\varepsilon_0}\ln\left(\frac{r^2+d^2-2rd\cos(\psi-\theta)}{a_1^2+d^2-2a_1d\cos(\psi-\theta)}\right). \tag{2}$$

If wire 2 is located at the origin, then (2) also holds, but the charges Q_1 and Q_2 are interchanged and the radius a_1 has to be replaced by a_2. Averaging (2) over the FDTD cell, yields the averaged potential, which is a function of the applied charges and the in-cell self and mutual capacitances C_{11} and C_{12}:

$$\langle V\rangle_1 = \frac{Q_1}{C_{11}} + \frac{Q_2}{C_{12}}. \tag{3}$$

Here averaging is defined as:

$$\langle V\rangle_1 = \int_{\Omega_1} V(r)\,r\,dr\,d\theta \Big/ \int_{\Omega_1} r\,dr\,d\theta \tag{4}$$

The subscript $\langle\rangle_1$ refers to the FDTD cell with wire 1 in the centre. In this case Ω_1 is the area of the FDTD cell, excluding the conductors. Similarly, expressions for the in-cell inductances are derived by starting from the static equation for currents on the two wires:

$$H_\theta = \frac{I_1}{2\pi\rho_1} + \cos\alpha\,\frac{I_2}{2\pi\rho_2}. \tag{5}$$

This equation, combined with Maxwell-Faraday's law, after similar steps as for the capacitances, yields the following equation:

$$L_{11}\frac{\partial I_1}{\partial t} + L_{12}\frac{\partial I_2}{\partial t} = -\frac{\partial\langle V\rangle_1}{\partial z} + \langle E_z\rangle_1. \tag{6}$$

Here:

$$L_{11} = \frac{\mu_0}{2\pi}\left\langle\ln\left(\frac{r}{a_1}\right)\right\rangle_1$$
$$L_{12} = \frac{\mu_0}{4\pi}\left\langle\ln\left(\frac{r^2+d^2-2rd\cos(\psi-\theta)}{a_1^2+d^2-2a_1d\cos(\psi-\theta)}\right)\right\rangle_1. \tag{7}$$

For homogeneous dielectric (non-magnetic) media, the in-cell inductance and capacitance are related in the following way:

$$L_{ij}C_{ij} = \mu_0\varepsilon_0\varepsilon_r. \tag{8}$$

Here ε_0 and μ_0 are the free space permittivity and permeability, while ε_r is the relative permittivity of the medium. After deriving the in-cell inductance and capacitance, the wires are coupled to the FDTD method with the following equations:

$$\frac{\partial\mathbf{I}}{\partial t} = -c^2\frac{\partial\mathbf{Q}}{\partial z} - \mathbf{L}^{-1}\begin{bmatrix}\langle E_z\rangle_1\\ \langle E_z\rangle_2\end{bmatrix}$$
$$\frac{\partial\mathbf{Q}}{\partial t} = -\frac{\partial\mathbf{I}}{\partial z}. \tag{9}$$

Here $\mathbf{Q}$ and $\mathbf{I}$ are the vectors carrying the p.u.l. charges and currents on each wire, while $\mathbf{L}$ is the matrix with all entries L_{ij}. E_z is the electric field component in the z-direction, coming from the FDTD solver.

III. Numerical Approximation of In-cell Parameters

Bérenger's method provides a very elegant and structured way to incorporate the effects of multiple wires in an FDTD cell into the FDTD method. However, there might be cases in which these analytical computations will not be possible. Examples

include inhomogeneous media or rectangular conductors. Moreover, Bérenger's analytical approximation of the in-cell parameters neglects certain interactions between conductors, which may become of importance for bundles with many closely spaced wires of various thicknesses. Hence, this section discusses a methodology to compute the in-cell inductance and capacitance numerically.

In general, the distribution of the potential V in a cross section perpendicular to the propagation direction of a transmission line (TL) satisfies the two-dimensional Laplace equation [2]:

$$\Delta V = 0. \tag{10}$$

To solve this equation, boundary conditions are required. To determine the in-cell parameter matrices, the contributions of the two terms in (2) are to be determined separately. This can be done by prescribing appropriate boundary conditions on the surfaces of the two wires. Let Γ_1 and Γ_2 be the boundaries of wires 1 and 2, with radii a_1 and a_2, respectively. To compute the first term in (2), at wire 1 a surface charge ρ_1 is prescribed, so that the following Neumann boundary condition holds and the total charge of the wire equals Q_1:

$$\left.\frac{\partial V}{\partial r}\right|_{\Gamma_1} = \frac{\rho_1}{\varepsilon} = \frac{Q_1}{2\pi\varepsilon a_1}. \tag{11}$$

The second wire is required to carry zero charge, i.e. $Q_2 = 0$. This can be achieved by either setting zero surface charge:

$$\left.\frac{\partial V}{\partial r}\right|_{\Gamma_2} = 0, \tag{12}$$

or by applying a condition such that the total charge equals zero:

$$Q_2 = \varepsilon \int_{\Gamma_2} \frac{\partial V}{\partial n} d\Gamma = 0. \tag{13}$$

The latter can be achieved by treating the second wire as a floating conductor, which can be implemented by assigning a very high permittivity to the interior of wire 2 [11]. Note that (12) is a special case of (13). To numerically compute the second term of (2), similar conditions as above should be applied, but with wires 1 and 2 interchanged.

Far away from the conductors the potential V behaves as:

$$V(r) \sim \log(r) + \gamma, \tag{14}$$

in which γ is a constant value that follows from requiring that the potential V is zero inside wire 1. In this paper, this requirement has been implemented by requiring the average of the potential V is zero around Γ_1:

$$\int_{\Gamma_1} V(r) d\Gamma = 0. \tag{15}$$

The numerical solution of (10) to (15) can be obtained by applying FEM [12] on an appropriate computational grid around the wires. This computational grid should be bounded by an artificial boundary far away from the wires. At this outer boundary, an absorbing boundary condition is applied that takes into account (14). This method is frequently used to compute per-unit-length (p.u.l.) TL parameters for MTL simulations [1]. Here it is used to compute the potential distribution inside the FDTD cell, from which the in-cell parameters can be derived.

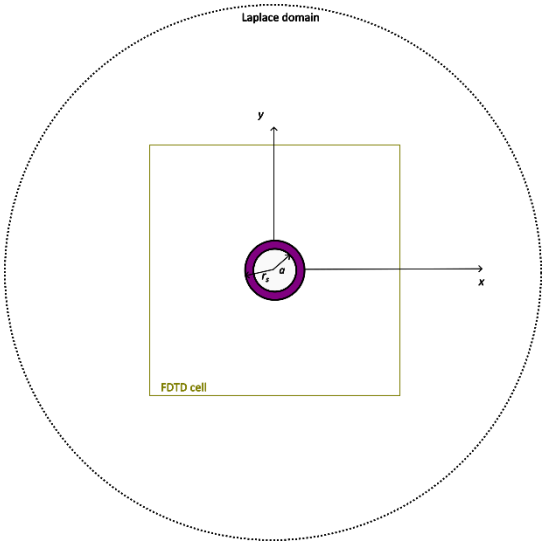

Fig. 2. Sketch of single wire with dielectric insulation (shown by purple area) inside an FDTD cell. Outer circle illustrates FEM domain.

A. *Wires in homogeneous media*

Equations (3) and (4) imply that it is required to calculate the averaged potential inside the FDTD cell, which directly relates to the in-cell capacitance. The main step in acquiring the contributions of each C_{ij} separately, boils down to subsequently using the correct boundary conditions. The following procedure is used to numerically determine the full in-cell capacitance matrix.

Start off by placing wire 1 in the centre of an FDTD cell, of which we denote the area with Ω_1, as shown in Fig. 1. Then apply the following steps:

a. Impose boundary condition (11) to wire 1, which prescribes the surface charge such that $Q_1 = 1$.
b. Apply either (12) or (13) to wire 2.
c. Solve the potential distribution.
d. Numerically integrate the potential over the FDTD cell and compute the averaged potential following (4).
e. Compute C_{11} from (3).
f. Repeat a-e with wires 1 and 2 interchanged to obtain C_{12}.

Next, place wire 2 in the centre of an FDTD cell of which we denote the area with Ω_2. Repeat the steps a through f above to compute C_{21} and C_{22}.

Once all capacitances have been determined, the corresponding in-cell inductances can be computed by (8), under the condition that the medium is homogeneous.

Since the potential distribution can be found numerically for any cabling configuration, not confined to cylindrical wires in homogeneous media, this method can be more broadly applied than Bérenger's analytical approach. The next subsection discusses what needs to be adapted to include wiring insulation.

B. *Inclusion of inhomogeneous dielectrics*

Dielectric insulation around wires will affect their potential distribution. In [10] inclusion of insulation in Bérenger's analytical formulation is discussed. For simplicity, consider the case of a single insulated wire as shown in Fig. 2. The wire has

radius a, while the dielectric has thickness $r_s - a$. The electric field here can be formulated with:

$$E_\rho = \begin{cases} \dfrac{Q}{2\pi\varepsilon_1\rho} & \rho \in \Omega_1 \\ \dfrac{Q}{2\pi\varepsilon_2\rho} & \rho \in \Omega_2. \end{cases} \tag{16}$$

Here Ω_1 is the purple area indicating dielectric material, and Ω_2 is the area between the boundary of the insulation and boundary of the FDTD cell. Integration of this electric field along ρ again yields the potential distribution:

$$V_r = \begin{cases} \dfrac{Q}{2\pi\varepsilon_1}\ln\left(r/a\right) & r < r_s \\ \dfrac{Q}{2\pi\varepsilon_1}\ln\left(r_s/a\right) + \dfrac{Q}{2\pi\varepsilon_2}\ln\left(r/r_s\right) & r > r_s. \end{cases} \tag{17}$$

The averaged potential can then be determined over the two regions Ω_1 and Ω_2 separately, or over the full FDTD cell at once. The two are related by:

$$\langle V_{tot}\rangle = \frac{r_s^2 - a^2}{r^2 - a^2}\langle V\rangle_{\Omega_1} + \frac{r^2 - r_s^2}{r^2 - a^2}\langle V\rangle_{\Omega_2}. \tag{18}$$

So, direct integration of the potential distribution equals the weighted sum of the separately averaged potentials, in which the weights are the ratio of the area of each region divided by the total area of the FDTD cell. From the total averaged potential, the total in-cell capacitance can again be computed. In case the FDTD cell is circular with radius r this would be equal to:

$$\begin{aligned} C_{tot} &= \frac{Q}{\langle V_{tot}\rangle} \\ &= \pi\left(r^2 - a^2\right)[B]^{-1} \\ B &= \frac{1}{\varepsilon_1}\left[\frac{r^2}{2}\ln\left(\frac{r_s}{a}\right) - \frac{r_s^2}{4} + \frac{a^2}{4}\right] \\ &\quad + \frac{1}{\varepsilon_2}\left[\frac{r^2}{2}\ln\left(\frac{r}{r_s}\right) - \frac{r^2}{4} + \frac{r_s^2}{4}\right]. \end{aligned} \tag{19}$$

Apart from analytically, such integration can again also be performed numerically. FEM solvers can easily take into account regions with varying dielectric media by requiring at the interfaces of the media that the normal components of the electric flux density across an interface between two media are continuous. At the interface of between two media with relative permittivity ε_1 and ε_2 the following holds:

$$\varepsilon_1\frac{\partial V_1}{\partial r} = \varepsilon_2\frac{\partial V_2}{\partial r}. \tag{20}$$

This has been implemented in the NLR in-house Laplace solver. Hence, the procedure to determine the in-cell capacitance matrix remains equal to what was discussed for the homogeneous case in Section IIIA.

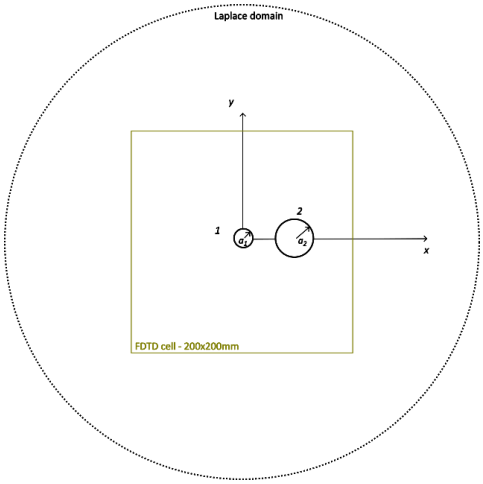

Fig. 3. Sketch of testcase with two wires with radii 1 mm and 10 mm, separated at 20 mm distance.

In-cell inductances are not derived from the electrical fields, but from the magnetic fields. Specifically they follow from (5). Actually, dielectric materials have no effect on the magnetic fields, hence also not on in-cell inductances. Therefore, the conclusion is that inductances should still be computed in the way it was done without dielectrics. In summary, the procedure to compute the in-cell inductances and capacitances for insulated wires is as follows:

1. Set up the Laplace solver with all dielectrics replaced by free space conditions (i.e. $\varepsilon_r = 1$).
    a. Follow the stepped procedure in Section IIIA to find the in-cell capacitance matrix under free space conditions.
    b. Compute the in-cell inductance matrix by (8).
2. Set up the Laplace solver with all dielectrics present.
    a. Follow the stepped procedure in Section IIIA to find the actual in-cell capacitance matrix.

Note that relation (8) will not hold anymore for the resulting in-cell inductance and capacitance matrices. Hence, the equations governing the coupling between FDTD and the wires (see (9)) need adaptation as well, since in the derivation of these relation (8) is used. For a single insulated wire, the new coupling equation should become:

$$\frac{\partial I}{\partial t} = -\frac{1}{LC}\frac{\partial Q}{\partial z} + \frac{1}{L}\langle E_z\rangle. \tag{21}$$

IV. Results

This section discusses the results of the testcase shown in Fig. 3, which is the exact same testcase that was also discussed by Bérenger in [8]. It considers two wires of radius 1 mm and 10 mm, separated by 20 mm. The FDTD cell has dimensions equal to 200 mm x 200 mm (see Fig. 2).

Table 1 shows the values of all four entries of the in-cell inductance and capacitance matrices, found when using Bérenger's analytical approximation and when using the numerical procedure of Section III. The 2nd and 3rd columns refer to the use of a floating conductor with (13) (implemented by using $\varepsilon_r = 1000$ inside the corresponding conductor) or by

Table 1. Obtained values for in-cell **C** and **L** matrices with Bérenger's analytical approach, or the numerical computations of Section III

Quantity	Bérenger	Floating conductor	Zero surface charge
C_{11}	13.13 pF	14.08 pF	12.39 pF
C_{12}	44.25 pF	43.99 pF	43.85 pF
C_{21}	44.33 pF	44.31 pF	36.06 pF
C_{22}	27.70 pF	28.79 pF	28.67 pF
L_{11}	847 nH	791 nH	898 nH
L_{12}	251 nH	253 nH	254 nH
L_{21}	251 nH	251 nH	309 nH
L_{22}	388 nH	387 nH	388 nH

Table 2. Obtained values for in-cell **C** and **L** matrices for thin wires with Bérenger's analytical approach, or the numerical computation of Section III

Quantity	Bérenger	Floating conductor	Zero surface charge
C_{11}	13.13 pF	13.15 pF	13.14 pF
C_{12}	44.25 pF	44.28 pF	44.20 pF
C_{21}	44.25 pF	44.29 pF	44.18 pF
C_{22}	13.13 pF	13.15 pF	13.13 pF
L_{11}	847 nH	846 nH	848 nH
L_{12}	251 nH	251 nH	252 nH
L_{21}	251 nH	251 nH	252 nH
L_{22}	847 nH	846 nH	847 nH

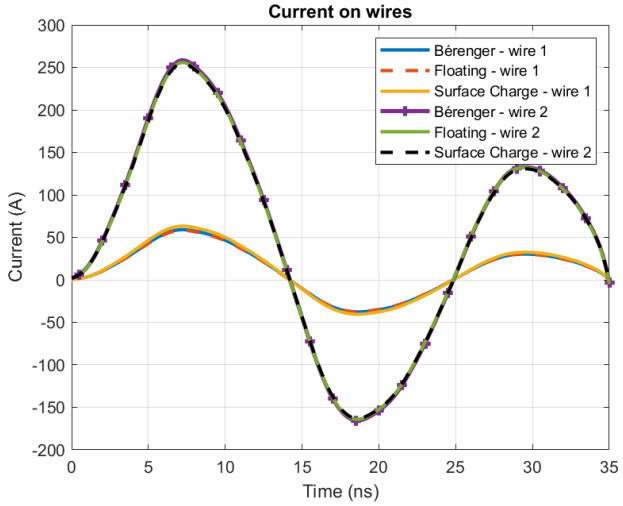

Fig. 4. Currents on wires 1 and 2 for testcase shown in Fig. 2, computed with UGR's FDTD solver by using either Bérenger's in-cell parameters, or the numerically determined in-cell parameters in Table 1.

using (12), respectively. In general, the resulting in-cell parameters are comparable, showing that numerical computation is a very suitable alternative. Fig. 4 shows the resulting currents on the two wires computed by FDTD when the wires are illuminated by a plane wave equal to that defined in [8]. Comparing Bérenger's analytical expressions versus the numerically found in-cell parameters, the results are nearly identical, and also correspond with the currents that Bérenger shows in his paper.

If the radius of the second wire would also be equal to 1 mm, the results for the in-cell parameters for the two compared

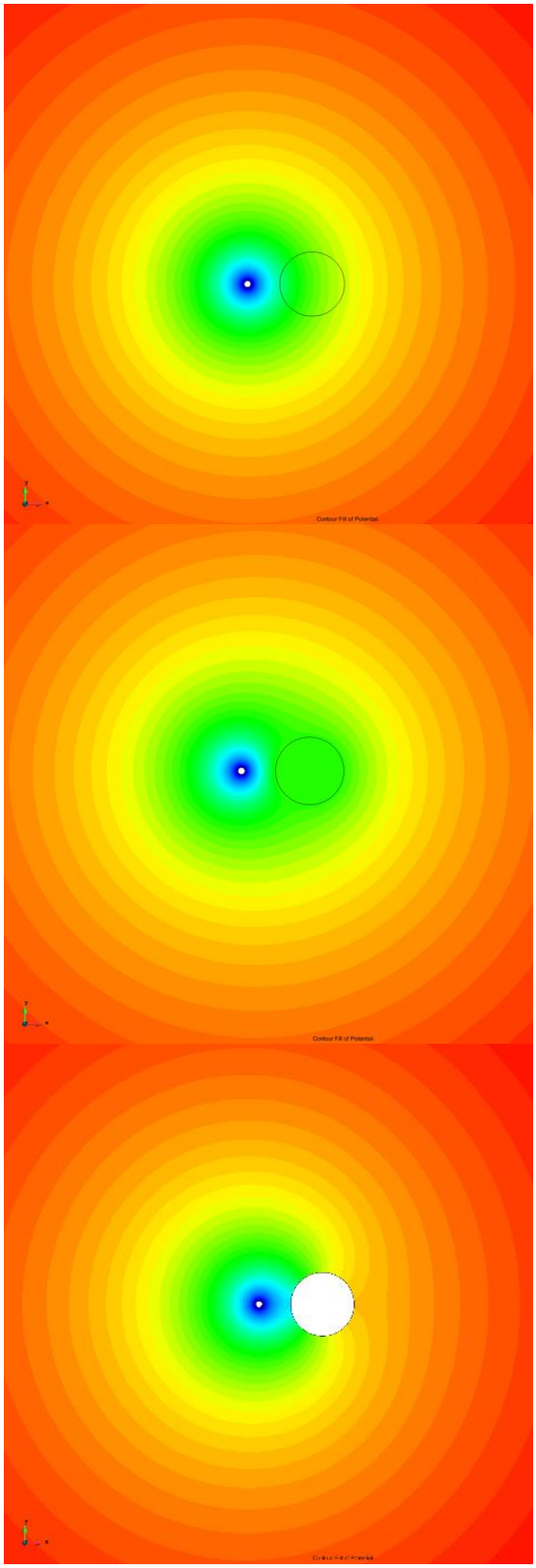

Fig. 5. Potential distribution used to determine L_{11} and C_{11}, wire 1 is located at the origin. Upper: obtained by Bérenger (2) with $Q_1 = 1$ and $Q_2 = 0$. Middle: obtained by NLR's Laplace solver with $Q_1 = 1$ in (11) for wire 1, and wire 2 as floating conductor. Bottom: obtained by NLR's Laplace solver with $Q_1 = 1$ in (11) for wire 1, and (12) for wire 2.

methods would even be closer (see Table 2). The differences that occur between the three approaches in Table 1, are mainly caused by the interactions between the wires. This is confirmed by the results shown in Fig. 5, which shows the potential distribution obtained with all three methods under discussion. The case shown, involves the distribution used for the computation of L_{11} and C_{11}, with wire 1 in the origin of the coordinate system, to which a charge of $Q_1 = 1$ is enforced. Zero charge is given to wire 2. Hence the potential distribution by Bérenger is given by the first term of equation (2). This potential distribution is shown in the upper part of Fig. 5, and is fully symmetrical around the angular spherical coordinate θ. Following Bérenger, there is no interaction between the two wires and the equipotential lines in this case continue through wire 2.

The numerical solutions do show that wire 2 should be affecting the equipotential lines, e.g. there should be some interaction between wires 1 and 2. The solution with Neumann boundary conditions on both wires, with zero surface charge applied to wire two, is shown in the lowest part of Fig. 5. The inside of wire 2 is shown white here, since the potential inside the conductor is not computed by the FEM. Clearly, condition (12) on wire 2 enforces the equipotential lines to be perpendicular to wire 2. This at its turn also yields a non-physical solution, since the result is a non-constant potential around the perimeter of wire 2, while this should be an equipotential body.

Finally, the middle part of Fig. 5 shows the solution in which wire two is a floating conductor, implemented by using higher permittivity. Clearly, the field lines are affected by the presence of the second wire, caused by the fact that in this case wire two is an equipotential body. And indeed, it satisfies relation (13) and carries zero net charge. Hence, this is the distribution that most accurately describes the effects of L_{11} and C_{11}. In Table 1, the variations in these in-cell parameters are largest, since varying the boundary condition on the thicker wire 2, has the most impact. The variations in the other three entries of the in-cell matrices are much less.

Finally, for the case including dielectrics shown in Fig. 2, let the wire radius a be 1 mm, and the dielectric thickness also 1 mm. For an FDTD cell of dimensions 15 mm x 15 mm the obtained in-cell parameters are shown in Table 3. This table shows the in-cell inductance and capacitance both with and without dielectrics. Naturally, the dielectrics have no impact on the inductance, but the capacitance clearly increases by 23% with the inclusion of dielectrics.

Table 3. In-cell inductance and capacitance for insulated wire

Quantity	Without dielectrics	With insulation
C_{11}	21.43 pF	26.39 pF
L_{11}	422 nH	422 nH

V. Conclusion

A methodology to numerically determine the in-cell inductance and capacitance matrices for multiple wires inside an FDTD cell is presented. The method provides a generalization to Bérenger's multiwire formalism, which is built upon analytical approximation of the in-cell parameters. The benefits of numerical computation are that any wiring configuration can be handled, including non-cylindrical conductors and inhomogeneous media. In case the effects of inhomogeneous dielectrics are to be included, the equations coupling the wires to the FDTD should be altered.

The results of the methodology have been compared to the original results of a testcase provided by Bérenger. Computed in-cell parameters match nearly perfectly for two thin wires with wide separation. For the testcase involving one thicker wire of 10 mm radius, some deviations start to occur. From the analysis of the potential distribution it was concluded that these differences are mainly caused by the missing interaction between the wires in Bérenger's analytical expressions.

Bérenger's multiwire formalism remains a very useful and powerful tool. However, the more generic method introduced in this paper may become very useful in case more complex bundles, with many wire sizes, dielectrics, and possibly non-cylindrical conductors such as busbars should be studied.

Acknowledgment

Funded by the European Union under GA no 101101961 - HECATE. Views and opinions expressed are however those of the author(s) only and do not necessarily reflect those of the European Union or Clean Aviation Joint Undertaking. Neither the European Union nor the granting authority can be held responsible for them. The project is supported by the Clean Aviation Joint Undertaking and its Members.

References

[1] SEMBA, "EMC Broadband Simulator," [Online]. Available: https://www.sembahome.org/

[2] C.R. Paul, *Analysis of Multiconductor Transmission Lines*, New York: John Wiley & Sons, 1994.

[3] J. Lansink Rotgerink, *Crosstalk Analysis in Aerospace Environments*, PhD Thesis, Enschede: University of Twente, 2022.

[4] J. Lansink Rotgerink, R. Serra and F. Leferink, "Multiconductor Transmission Line Modeling of Crosstalk Between Cables in the Presence of Composite Ground Planes," *IEEE Transactions on Electromagnetic Compatibility*, vol. 63, no. 4, pp. 1231–1239, Dec. 2020.

[5] J. Lansink Rotgerink, "Radiated Emissions from Power Feeders for Electric Propulsion in Aircraft," *2022 International Symposium on Electromagnetic Compatibility (EMC Europe)*, Gothenburg, Sweden, Sept. 2022, pp. 490-495.

[6] G. Gutierrez, D. Romero, M. Cabello, E. Pascual-Gil, L. Angulo, D. Gomez and S. Garcia, "On the Design of Aircraft Electrical Structure Networks," *IEEE Transactions on Electromagnetic Compatibility*, vol. 58, no. 2, pp. 401–408, Apr. 2016.

[7] R. Holland and L. Simpson, "Finite-Difference Analysis of EMP Coupling to Thin Struts and Wires," *IEEE Transactions on Electromagnetic Compatibility*, vol. EMC-23, no. 2, pp. 88–97, May 1981.

[8] J. Bérenger, "A Multiwire Formalism for the FDTD method," *IEEE Transactions on Electromagnetic Compatibility*, vol. 42, no. 3, pp. 257–264, Aug. 2000.

[9] M. Feliziani and F. Maradei, "Full-wave analysis of shielded cable configurations by the FDTD method," *IEEE Transactions on Magnetics*, vol. 38, no. 2, pp. 761–764, March 2002.

[10] C. Guiffaut, N. Rouvrais, A. Reineix, "Insulated Oblique Thin Wire Formalism in the FDTD Method," *IEEE Transactions on Electromagnetic Compatibility*, vol. 59, no. 5, pp. 1532–1540, Oct. 2017.

[11] W.N. Fu, S.L. Ho, S. Niu, J. Zhu, "Comparison Study of Finite Element Methods to Deal With Floating Conductors in Electric Field," *IEEE Transactions on Magnetics*, vol. 48, no. 2, pp. 351–354, Feb. 2012.

[12] J. Jin, *The Finite Element Method in Electromagnetics*, Wiley-IEEE Press, April 2014.